DEBRIS SENSING BASED ON LEO CONSTELLATION: AN INTERSATELLITE CHANNEL PARAMETER ESTIMATION APPROACH

Yuan Liu, M. R. Bhavani Shankar, Linlong Wu, Björn Ottersten

Interdisciplinary Centre for Security, Reliability and Trust (SnT), University of Luxembourg
Email: {yuan.liu, bhavani.shankar, linlong.wu, bjorn.ottersten }@uni.lu

ABSTRACT

Space debris detection and tracking, a key enabler for Space Situational Awareness (SSA), poses two inherent challenges: (1) small-sized targets (e.g., $1-10$ cm) posing detection difficulties for conventional ground-based radars (GBRs) and optical measurements; (2) large number resulting in a costly tracking exercise. To address these, this work utilizes intersatellite link (ISL) in the emerging low earth orbit (LEO) constellations to opportunistically sense debris. The spatially dense-distributed debris is modeled as a cluster to reduce the number of quantities estimated. Using a stochastic geometry-based channel model, a nested expectation-based SAGE^2 is proposed, building on space-alternative-generation-estimation-maximization (SAGE) to estimate the cluster-based channel parameters. Finally, the debris clusters are localized using the ISL forming a bistatic sensing setup. Simulation results validate the proposed approach and show the proposed SAGE^2 is faster than the conventional SAGE in clustered multipath channels.

***Index Terms*—** Channel parameter estimation, Debris sensing, LEO Constellation, SAGE, stochastic geometry.

1. INTRODUCTION

Low earth orbit (LEO) satellite constellations, like StarLink and OneWeb, are key enablers in the space-aided next-generation communication systems [1, 2]. However, with a large number of assets in space, debris has become imminent regarding the security and robustness of the satellites. An additional issue is a large number of tiny debris from collisions, e.g., the hyper-velocity LEO collision events (Iridium 33 and Cosmos 2251) resulted in thousands of untrackable objects less than 10 cm in diameter [3]. Detecting debris and estimating its trajectory is central towards avoiding and creating additional debris. However, the detection of small-sized objects using ground-based radars (GBRs) and optical measurements becomes difficult due to the typical $500-1000$ km detection distance of LEO debris. Hence, space-based measurements are needed for detecting small debris. However, a separate stand-alone debris detection system is costly and unrealistic given the extent of space.

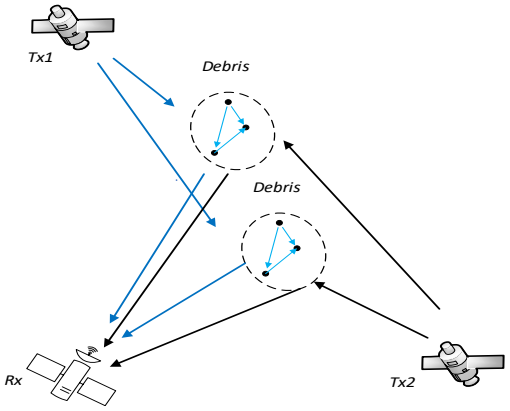

Fig. 1: Debris sensing based on ISL.

We consider debris detection to be a twofold system. Firstly, the existing large LEO constellations are additionally used as bistatic sensing systems for opportunistic detection. This would not use extra resources of the inter-satellite communications, and it serves as preliminary localization. Then, the specific threatening debris will be further refined using a dedicated monostatic setup. This paper introduces the first step, i.e., the intersatellite links (ISL) based opportunistic sensing. A typical hardware architecture of the integrated sensing and communication (ISAC) satellite system is described in [4], where ISLs are used for debris detection. In particular, Fig. 1 depicts the opportunistic use of ISL for debris detection. This context [4] mainly analyzes the satellite density needed and the coverage of detection based on link budget calculation. However, the estimation is not mentioned.

In this work, we convert the debris sensing to parameter estimation of the non-line-of-sight (NLoS) ISLs. There are various high-resolution channel parameter estimation algorithms, such as spectral estimation [5, 6], subspace-based estimation [7, 8], and deterministic parameter estimation [9], where the iterative expectation-maximization (EM) using maximum likelihood estimation (MLE) are popular for parameter estimations of multipath channel. The space-alternative-generation-EM (SAGE) is an acceleration struc-

This work was supported by the Luxembourg National Research Fund (FNR) through the BRIDGES project MASTERS under grant BRIDGES2020/IS/15407066 and the CORE INTER project SENCOM under grant C20/IS/14799710.

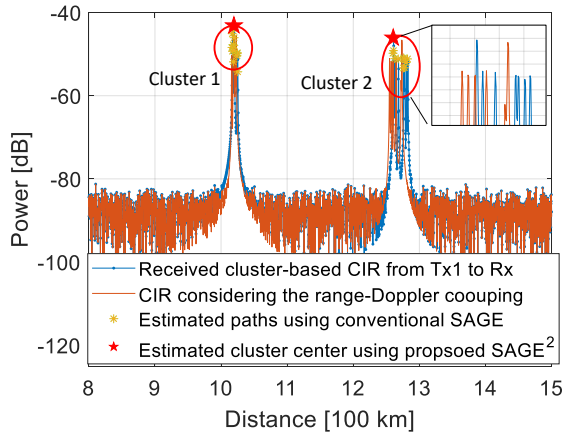

Fig. 2: Cluster-based CIRs and effects of cluster and range-Doppler coupling in CIR; scenario details in Fig. 3 (a); the estimation using will be discussed in the simulation part.

ture of EM [10, 11], where parameter subsets are alternatively estimated in each iteration until convergence. Most of the SAGE-based channel estimation methods assume the multipaths are resolvable and estimate individual paths sequentially, however, it can lead to errors due to model mismatches in cases of multipath correlations [12].

Considering the large number of dense-distributed debris in our application, the assumption of conventional SAGE is not realistic. Furthermore, estimating the large number of multipaths is time costly and not suitable for fast-time-varying satellite channels. To address these, we model the spatial dense-distributed debris to be clustered. Then, we propose a nested expectation (E)-based SAGE (SAGE^2) algorithm for the cluster-based channel model, where the path parameters of the centric path in each cluster are estimated, and other multipaths are statistically represented, hence estimating fewer paths and reducing the iterations than the conventional SAGE algorithm. By using the estimated channel parameters, e.g., the propagation delay between different transmitter (Tx) and receiver (Rx) pairs, the debris can be localized using classical time-difference-of-arrival (TDoA) methods [13].

2. SIGNAL MODEL

A scenario with two Tx satellites and an Rx satellite is illustrated in Fig. 1. ISLs are established between satellites and such links can also be used to illuminate debris in the field of view. In the absence of other scatterers in space, the NLoS path offers information about the debris. While any satellite can be Tx/ Rx based on the protocol, the identified Rx satellite receives signals containing multipath information of debris from the adjacent Tx satellites and acts as the data fusion center for ease of comprehension. This example scenario is generalized to a multistatic sensing system where M Tx satellites and one Rx satellite are used to sense the $L \geq 1$ debris clusters. For this initial work, no scattering among different debris clusters is assumed, but bounces within a cluster are considered. This leads to diffuse multipaths, i.e. clustering paths are similar in the amplitude and range domains of channel impulse response (CIR) as shown in Fig. 2.

Let $l_K \geq 1$ denote the number of scattering paths for the lth cluster ($l \in [1, L]$). Further, letting h_{l_c} denote the path corresponding to the centroid of the lth cluster (or the equivalent central path), the channel of the l_kth ($l_k \in [1, l_K]$) debris can be characterized as amplitude and phase perturbed versions of the of h_{l_c}, i.e.,

$$h_{l,l_k}(t) = h_{l_c}(t)\Delta h_{l,l_k} = h_{l_c}(t)(1+\Delta\alpha_{l_k})e^{j\Delta\varphi_{l_k}}, \quad (1)$$

where $\Delta\alpha_{l_k}$ and $\Delta\varphi_{l_k}$ follow the normal distribution $N(0,\sigma_1^2)$ and $N(0,\sigma_2^2)$, respectively, where σ_1 and σ_2 are the standard deviations of amplitude uncertainty and phase shift. Considering a sampling rate f_s with P samples in a burst (or a frame defined according to the standard), the baseband equivalent signal model of $h_{l_c}(t)$ is

$$h_{l_c}(p) = \alpha_{l_c} \underbrace{e^{-j2\pi f_s p \tau_{l_c}}}_{range} \underbrace{e^{j2\pi \frac{f_c}{f_s}\frac{v_{l_c}^{\text{tx}}+v_{l_c}}{c}p}}_{Range-Doppler-coupling}, \quad (2)$$

with the sampling index $p = 1, 2, ..., P$ and the α_{l_c} is the receiving power as

$$\alpha_{l_c} = P_t G_t G_r S_{l_c} \frac{c^2}{(4\pi f_c d_{l_c}^{\text{td}} d_{l_c}^{\text{rd}})^2}, \quad (3)$$

where P_t, G_t, G_r, S_{l_c}, f_c denote the transmitted power, Tx antenna gain, Rx antenna gain, scattering coefficient, carrier frequency, respectively, $d_{l_c}^{\text{td}}$ and $d_{l_c}^{\text{rd}}$ are distances from Tx to debris and from debris to Rx, respectively, $\tau_{l_c} = (d_{l_c}^{\text{td}} + d_{l_c}^{\text{rd}})/c$ is propagation delay, c is light velocity, v_{l_c} is the projection of the debris velocity on the transmission path and, similarly, $v_{l_c}^{\text{tx}}$ is the projection of the Tx velocity on the path.

The resulting NLoS channel is the superposition of individual components from all the clusters, and is denoted as

$$h_{\text{NLoS}}(p) = \sum_{l=1}^{L}\sum_{l_k=1}^{l_K} h_{l,l_k}(p) + z(p) = \sum_{l=1}^{L} h_l(p) + z(p), \quad (4)$$

where $z(p)$ is the white Gaussian noise.

Discussion of range-Doppler coupling: The channel in (2) has two exponentials, the first of which is due to range. Further, since the constellation and debris are moving fast, the second term indicating the range-Doppler coupling effect can impact the accuracy of distance estimation [14, 15]. An example of cluster 2 is illustrated in the orange curve of Fig. 2, where a relative velocity of debris is 5 km/s and the error in delay estimation is about 2.6 km. Addressing this coupling could be attempted using waveform design, and multiple frames of data. However, for simplicity, we would pursue

the estimation of approximate delay due to coupling without additional processing. This serves as preliminary localization, which can be further refined for specific *threatening* debris using a dedicated monostatic set-up.

3. CHANNEL PARAMETERS ESTIMATION ALGORITHM

Let $\mathbf{h}_{\text{NLoS}} = [h_{\text{NLoS}}(1), h_{\text{NLoS}}(2), \ldots, h_{\text{NLoS}}(P)]^T$ denote the stacking of (4) over the P length burst, where $(\cdot)^T$ and $(\cdot)^H$ denote the transpose and the conjugate transpose of a matrix or vector. The received signal consists of the multipaths from L clusters, following the concept of EM, this incomplete data $\mathbf{h}_{\text{NLoS}} \in \mathbb{C}^{P\times 1}$ can be decomposed into L complete data $\mathbf{h}_l \in \mathbb{C}^{P\times 1}$ as

$$\begin{aligned}\mathbf{h}_{\text{NLoS}} &= \sum_{l=1}^{L}\mathbf{h}_l = \sum_{l=1}^{L}\left(\sum_{l_k=1}^{l_K}\mathbf{h}_{l,l_k} + \beta_l\mathbf{z}\right)\\ &= \sum_{l=1}^{L}\left(\sum_{l_k=1}^{l_K}\mathbf{h}_{l_c}\odot\Delta\mathbf{h}_{l,l_k} + \beta_l\mathbf{z}\right),\end{aligned} \tag{5}$$

where the entries of the vector $\mathbf{h}_{l_c} \in \mathbb{C}^{P\times 1}$ defined in (5) and the entries of the vector $\Delta\mathbf{h}_{l,l_k} \in \mathbb{C}^{P\times 1}$ are defined as $\Delta h_{l,l_k}$ in (1), $\odot$ denotes the Hadamard products, $\mathbf{z} \in \mathbb{C}^{P\times 1}$ is white Gaussian noise with the variance being σ_0^2, and $\sum_{l=1}^{L}\beta_l = 1$ to satisfy the conservation of noise variance between complete data and incomplete data.

The conventional SAGE algorithm works when the incomplete data is composed of independent and resolvable multipaths, i.e., (5) can be thought of $\sum_{l=1}^{L} l_k$ paths. However, in this case, the paths within the cluster are correlated in (1) and are not necessarily resolvable. Further, we have,

$$\begin{aligned}\mathbf{h}_l &= \sum_{l_k=1}^{l_K}\mathbf{h}_{l_c}\odot\Delta\mathbf{h}_{l,l_k} + \beta_l\mathbf{z} = l_K\mathbf{h}_{l_c}\odot\left[\frac{1}{l_K}\sum_{l=1}^{L}\Delta\mathbf{h}_{l,l_k}\right]\\ \mathbf{h}_l &\approx l_K\mathbf{h}_{l_c}\odot\mathbb{E}\left[\Delta\mathbf{h}_{l,l_k}\right] + \beta_l\mathbf{z},\end{aligned} \tag{6}$$

where the sum is replaced by the expectation $\mathbb{E}(\cdot)$, under the assumption of the large number of paths within a cluster. As discussed in Section I, the current work omits the range-Doppler term in (2), leading to

$$\mathbf{h}_{l_c} \approx \alpha_{l_c}\mathbf{a}(\tau_{l_c}), \tag{7}$$

where α_{l_c} is defined in (3) and the delay vector $\mathbf{a}(\tau_l) \in \mathbb{C}^{P\times 1} = [e^{-j2\pi f_s 1\tau_{l_c}} e^{-j2\pi f_s 2\tau_{l_c}} \ldots e^{-j2\pi f_s P\tau_{l_c}}]^T$. Further,

$$\begin{aligned}\mathbb{E}\left[\Delta\mathbf{h}_{l,l_k}\right] &= \mathbb{E}[\underbrace{e^{j\Delta\varphi_{l_k}}}_{f(\Delta\varphi_{l_k})} + \underbrace{\Delta\alpha_{l_k}e^{j\Delta\varphi_{l_k}}}_{g(\Delta\varphi_{l_k})}]\\ &= \mathbb{E}\left[f(\Delta\varphi_{l_k})\right] + \mathbb{E}\left[g(\Delta\varphi_{l_k})\right].\end{aligned} \tag{8}$$

The expectation of $f(\Delta\varphi_{l_k})$ is a typical characteristic function of the Gaussian distribution [16] as

$$\mathbb{E}_{f(\Delta\varphi_{l_k})} = e^{-\frac{1}{2}\sigma_2^2}, \tag{9}$$

where the variance σ_2^2 is defined in (1). Because $\Delta\alpha_{l_k}$ and $\Delta\varphi_{l_k}$ are independent and follow the normal distribution,

$$\mathbb{E}_{g(\Delta\varphi_{l_k})} = \mathbb{E}_{\Delta\alpha_{l_k}}\mathbb{E}_{e^{j\Delta\varphi_{l_k}}} = 0, \tag{10}$$

where $\mathbb{E}_{\Delta\alpha_{l_k}} = 0$. Substituting (7) and (8) into (6), we can characterize the channel of the lth cluster as

$$\mathbf{h}_l = l'_k l_K\alpha_{l_c}\mathbf{a}(\tau_{l_c}) + \beta_l\mathbf{z} = l'_k\tilde{\mathbf{h}}_l + \beta_l\mathbf{z}, \tag{11}$$

where $l'_k = e^{-\frac{1}{2}\sigma_2^2}$ and $\tilde{\mathbf{h}}_l = l_K\alpha_{l_c}\mathbf{a}(\tau_{l_c})$, the parameters to be estimated are $\boldsymbol{\theta}_l = [\tau_{l_c}, \alpha_{l_c}, l_K]$.

While the MLE of $\boldsymbol{\theta}_l$ for the complete data is $\arg\max_{\boldsymbol{\theta}_l}\{\mathbf{h}_l(\boldsymbol{\theta}_l)\}$, the quantity $\mathbf{h}_l$ is not observable. However, the conditional expectation $\mathbb{E}[\mathbf{h}_l(\boldsymbol{\theta}_l)|\mathbf{H}_{\text{NLoS}}(\hat{\boldsymbol{\theta}}_l), \hat{\boldsymbol{\theta}}_l]$, has the same dependence on $\boldsymbol{\theta}_l$ as the original MLE function, hence it is used to estimate $\hat{\mathbf{h}}_l$. The iterative EM framework can be utilized with the ith iteration comprising the following steps:

- E-step: With an initialization $\boldsymbol{\theta}_l^{(0)}$ and following [17], closed-form expression of $\mathbb{E}[\mathbf{h}_l(\boldsymbol{\theta}_l)|\mathbf{H}_{\text{NLoS}}(\hat{\boldsymbol{\theta}}_l), \boldsymbol{\theta}_l]$ is,

$$\hat{\mathbf{h}}_l^{(i)} = l'_k\tilde{\mathbf{h}}_l(\boldsymbol{\theta}_l^{(i-1)}) + \beta_l\left(\mathbf{h}_{\text{NLoS}} - \sum_{l=1}^{L} l'_k\tilde{\mathbf{h}}_l(\boldsymbol{\theta}_l^{(i-1)})\right). \tag{12}$$

- M-step: Obtaining the parameters as

$$\boldsymbol{\theta}_l^{(i)} = \arg\min_{\boldsymbol{\theta}_l}\frac{\left(\hat{\mathbf{h}}_l^{(i)} - l'_k\tilde{\mathbf{h}}_l(\boldsymbol{\theta}_l)\right)\left(\hat{\mathbf{h}}_l^{(i)} - l'_k\tilde{\mathbf{h}}_l(\boldsymbol{\theta}_l)\right)^H}{\beta_l\sigma_0^2} \text{ i.e.,}$$

$$\begin{aligned}\tau_{l_c}^{(i)} &= \arg\min_{\tau_{l_c}}\frac{1}{\beta_l\sigma_0^2}\left(\hat{\mathbf{h}}_l^{(i)} - l'_k\tilde{\mathbf{h}}_l([\alpha_{l_c}^{(i-1)}, \tau_{l_c}, l_K^{(i-1)}])\right)\\ &\quad\times\left(\hat{\mathbf{h}}_l^{(i)} - l'_k\tilde{\mathbf{h}}_l([\alpha_{l_c}^{(i-1)}, \tau_{l_c}, l_K^{(i-1)}])\right)^H.\end{aligned} \tag{13}$$

$$\begin{aligned}\alpha_{l_c}^{(i)} &= \left(\tilde{\mathbf{h}}_l([\alpha_{l_c}, \tau_{l_c}^{(i)}, l_K^{(i-1)}])^H\tilde{\mathbf{h}}_l([\alpha_{l_c}, \tau_{l_c}^{(i)}, l_K^{(i-1)}])\right)^{-1}\\ &\quad\times\tilde{\mathbf{h}}_l([\alpha_{l_c}, \tau_{l_c}^{(i)}, l_K^{(i-1)}])^H\hat{\mathbf{h}}_l^{(i)}.\end{aligned} \tag{14}$$

$$\begin{aligned}l_K^{(i)} &= \arg\min_{l_K}\frac{1}{\beta_l\sigma_0^2}\left(\hat{\mathbf{h}}_l^{(i)} - l'_k\tilde{\mathbf{h}}_l([\alpha_{l_c}^{(i)}, \tau_{l_c}^{(i)}, l_K])\right)\\ &\quad\times\left(\hat{\mathbf{h}}_l^{(i)} - l'_k\tilde{\mathbf{h}}_l([\alpha_{l_c}^{(i)}, \tau_{l_c}^{(i)}, l_K])\right)^H.\end{aligned} \tag{15}$$

In practice, we need to have a phase search to match the exact path in (15) to estimate $l_K^{(i)}$ and obtain MLE.

4. SIMULATION

Simulation scenario and CIRs: We use 1 Rx (data fusion center) and 3 adjacent Txs in the constellation to sense debris in

Fig. 3: (a) The opportunistic multipaths propagation between Txs and Rx, where the blue, green, and yellow dash lines are Tx1-Rx, Tx2-Rx, and Tx3-Rx links, respectively. (b) Positioning result of the cluster center. The scales for (a) and (b) are $1:100\ km$. (c) Comparison with conventional SAGE: iteration times

Table 1: Simulation configurations

Configurations	Values
Simulation range [km^2]	1000^2
Central frequency f_c [GHz]	14 GHz
Sampling rates f_s [MHz]	1
Sampling number P	7001
EIRP [dBW]	34
Receiving antenna gain [dB]	30
SNR [dB]	40
Tx velocity	$[0, -3]\ km/s$
Debris velocity	$[5, 0]\ km/s$
Number of debris in Cluster 1	25
Number of debris in Cluster 2	15

a region of $1000 \times 1000\ km^2$ and a snapshot of the constellation is shown in Fig. 3 (a), where two debris clusters are considered. Other important simulation parameters are shown in Table 1. In this simulation, the stochastic graph theory [18] is utilized to generate the opportunistic multipaths of the ISLs, hence in Fig. 3 (a), we can observe that random propagation from Tx to debris, and from debris to Rx. The received CIR from Tx1 to Rx is also illustrated in Fig. 2, where the two clusters are observed clearly.

Path estimation and localization: The estimated results are also shown in Fig. 2, where the estimated paths of cluster centroid using the proposed SAGE^2 are denoted as red stars, and estimated paths using conventional SAGE are denoted as yellow dots. Typically, the scatterer localization based on the conventional SAGE algorithm requires further clustering algorithms [19, 20], because of the large number of estimated paths. In the proposed method, the cluster centroid is estimated, therefore it can be directly used for localization. The proposed SAGE^2 is well suited to this constellation-based debris sensing. Using multiple adjacent Txs of the Rx, the conventional time-of-arrival can be used for debris localization [21]. The localization results are shown in Fig. 3 (b), where the cluster is positioned.

Convergence analysis: The comparison between the proposed SAGE^2 and the conventional SAGE is shown in Fig. 3 (c). The conventional SAGE algorithm requires prior information on the number of paths in the channel. The convergent iteration times with the pre-set estimated paths of 5, 15, and 35 are shown in the blue cures in Fig. 3 (c). It shows that the incorrect number of estimated path settings will lead to local optima. In our proposed method, the prior information on the number of clusters is much easier to obtain. Besides, the SAGE^2 can also predict the number of paths in each cluster, e.g., the estimated paths of cluster 1 and cluster 2 are 20 and 24. respectively. With correct prior information, both methods can reach optimal results: the conventional SAGE provides all the paths at a higher computation, while the proposed SAGE^2 gives the cluster centroid at a lower time.

5. CONCLUSION

This work proposes an opportunistic debris-sensing approach based on channel parameter estimation using the ISLs in LEO constellations. In this approach, the debris is modeled as clusters and the proposed SAGE^2 method is used to estimate the parameters of the cluster-based channel and localize the centroid of the debris cluster based on the estimated delay information among different Tx-debris-Rx links. The SAGE^2 is tested using a stochastic channel model with multiple clusters, as well as the convergence comparison with the conventional SAGE algorithm. The results show that the proposed approach works well in debris center localization with fewer iterations for convergence. The output of the proposed method can be further used by dedicated mechanisms for further identification and accurate tracking of threatening debris.

6. REFERENCES

[1] S. Liu, Z. Gao, Y. Wu, D. W. Kwan Ng, X. Gao, K.-K. Wong, S. Chatzinotas, and B. Ottersten, "LEO Satellite Constellations for 5G and Beyond: How Will They Reshape Vertical Domains?" *IEEE Communications Magazine*, vol. 59, no. 7, pp. 30–36, 2021.

[2] X. Liu, T. Ma, Z. Tang, X. Qin, H. Zhou, and X. S. Shen, "Ultrastar: A lightweight simulator of ultra-dense LEO satellite constellation networking for 6G," *IEEE/CAA Journal of Automatica Sinica*, vol. 10, no. 3, pp. 632–645, 2023.

[3] M. Matney, "Small debris observations from the iridium 33/cosmos-2251 collision," *Orbital Debris Quarterly News*, vol. 14, no. 2, pp. 6–8, 2010.

[4] A. Anttonen, M. Kiviranta, and M. Höyhtyä, "Space debris detection over intersatellite communication signals," *Acta Astronautica*, vol. 187, pp. 156–166, 2021.

[5] R. Schmidt, "Multiple emitter location and signal parameter estimation," *IEEE Transactions on Antennas and Propagation*, vol. 34, no. 3, pp. 276–280, 1986.

[6] W.-X. Long, R. Chen, M. Moretti, W. Zhang, and J. Li, "Joint OAM radar-communication systems: Target recognition and beam optimization," *IEEE Transactions on Wireless Communications*, vol. 22, no. 7, pp. 4327–4341, 2023.

[7] R. Roy and T. Kailath, "ESPRIT-estimation of signal parameters via rotational invariance techniques," *IEEE Transactions on Acoustics, Speech, and Signal Processing*, vol. 37, no. 7, pp. 984–995, 1989.

[8] J. Zhang, D. Rakhimov, and M. Haardt, "Gridless channel estimation for hybrid mmWave MIMO systems via Tensor-ESPRIT algorithms in DFT beamspace," *IEEE Journal of Selected Topics in Signal Processing*, vol. 15, no. 3, pp. 816–831, 2021.

[9] A. P. Dempster, N. M. Laird, and D. B. Rubin, "Maximum likelihood from incomplete data via the EM algorithm," *Journal of the Royal Statistical Society: series B (methodological)*, vol. 39, no. 1, pp. 1–22, 1977.

[10] B. Fleury, M. Tschudin, R. Heddergott, D. Dahlhaus, and K. Ingeman Pedersen, "Channel parameter estimation in mobile radio environments using the SAGE algorithm," *IEEE Journal on Selected Areas in Communications*, vol. 17, no. 3, pp. 434–450, 1999.

[11] J. Hong, J. Rodríguez-Piñeiro, X. Yin, and Z. Yu, "Joint channel parameter estimation and scatterers localization," *IEEE Transactions on Wireless Communications*, vol. 22, no. 5, pp. 3324–3340, 2023.

[12] D. Shutin and B. H. Fleury, "Sparse variational bayesian sage algorithm with application to the estimation of multipath wireless channels," *IEEE Transactions on Signal Processing*, vol. 59, no. 8, pp. 3609–3623, 2011.

[13] X. Ye, J. Rodríguez-Piñeiro, Y. Liu, X. Yin, and A. Pérez Yuste, "A novel experiment-free site-specific TDOA localization performance-evaluation approach," *Sensors*, vol. 20, no. 4, p. 1035, 2020.

[14] R. J. Fitzgerald, "Effects of range-doppler coupling on chirp radar tracking accuracy," *IEEE Transactions on Aerospace and Electronic Systems*, vol. AES-10, no. 4, pp. 528–532, 1974.

[15] T. Feuillen, A. Mallat, and L. Vandendorpe, "Stepped frequency radar for automotive application: Range-Doppler coupling and distortions analysis," in *MILCOM 2016 - 2016 IEEE Military Communications Conference*, 2016, pp. 894–899.

[16] T. Anderson, *AN INTRODUCTION TO MULTIVARIATE STATISTICAL ANALYSIS, 3RD ED*. Wiley India Pvt. Limited, 2009. [Online]. Available: https://books.google.lu/books?id=1iF0CgAAQBAJ

[17] M. Feder and E. Weinstein, "Parameter estimation of superimposed signals using the EM algorithm," *IEEE Transactions on Acoustics, Speech, and Signal Processing*, vol. 36, no. 4, pp. 477–489, 1988.

[18] Y. Liu, X. Yin, X. Ye, Y. He, and J. Lee, "Embedded propagation graph model for reflection and scattering and its millimeter-wave measurement-based evaluation," *IEEE Open Journal of Antennas and Propagation*, vol. 2, pp. 191–202, 2021.

[19] C. Huang, A. F. Molisch, Y.-A. Geng, R. He, B. Ai, and Z. Zhong, "Trajectory-joint clustering algorithm for time-varying channel modeling," *IEEE Transactions on Vehicular Technology*, vol. 69, no. 1, pp. 1041–1045, 2019.

[20] Y. Liu, L. Wu, M. Alaee-Kerahroodi, and B. S. M. R, "A 3D indoor localization approach based on spherical wave-front and channel spatial geometry," in *2022 IEEE 12th Sensor Array and Multichannel Signal Processing Workshop (SAM)*, 2022, pp. 101–105.

[21] Y. Chan and K. Ho, "A simple and efficient estimator for hyperbolic location," *IEEE Transactions on Signal Processing*, vol. 42, no. 8, pp. 1905–1915, 1994.